Remote Sensing of Environment 190 (2017) 247–259

Contents lists available at ScienceDirect

Remote Sensing of Environment

journal homepage: www.elsevier.com/locate/rse

Comparison of commonly-used microwave radiative transfer models for snow remote sensing

Alain Royer [a,b,*], Alexandre Roy [a,b], Benoit Montpetit [a,1], Olivier Saint-Jean-Rondeau [a,b], Ghislain Picard [c], Ludovic Brucker [d,e], Alexandre Langlois [a,b]

[a] Centre d'Applications et de Recherches en Télédétection (CARTEL), Université de Sherbrooke, 2500 boul. Université, Sherbrooke, QC, Canada J1K 2R1
[b] Centre d'Études Nordiques, Québec, Canada
[c] Université Grenoble Alpes - CNRS, LGGE UMR5183, 38041 Grenoble, France
[d] NASA Goddard Space Flight Center, Cryospheric Sciences Laboratory, Code 615, Greenbelt, MD 20771, USA
[e] Universities Space Research Association, Goddard Earth Sciences Technology and Research, Columbia, MD 21046, USA

ARTICLE INFO

Article history:
Received 23 September 2016
Received in revised form 19 December 2016
Accepted 30 December 2016
Available online xxxx

Keywords:
Snow microwave-emission model
Snow microstructure
Radiative transfer model
Canada
Ground-based measurements
Brightness temperature

ABSTRACT

This paper reviews four commonly-used microwave radiative transfer models that take different electromagnetic approaches to simulate snow brightness temperature (T_B): the Dense Media Radiative Transfer - Multi-Layer model (DMRT-ML), the Dense Media Radiative Transfer - Quasi-Crystalline Approximation Mie scattering of Sticky spheres (DMRT-QMS), the Helsinki University of Technology n-Layers model (HUT-nlayers) and the Microwave Emission Model of Layered Snowpacks (MEMLS). Using the same extensively measured physical snowpack properties, we compared the simulated T_B at 11, 19 and 37 GHz from these four models. The analysis focuses on the impact of using different types of measured snow microstructure metrics in the simulations. In addition to density, snow microstructure is defined for each snow layer by grain optical diameter (Do) and stickiness for DMRT-ML and DMRT-QMS, mean grain geometrical maximum extent (D_{max}) for HUT n-layers and the exponential correlation length for MEMLS. These metrics were derived from either in-situ measurements of snow specific surface area (SSA) or macrophotos of grain sizes (D_{max}), assuming non-sticky spheres for the DMRT models. Simulated T_B sensitivity analysis using the same inputs shows relatively consistent T_B behavior as a function of Do and density variations for the vertical polarization (maximum deviation of 18 K and 27 K, respectively), while some divergences appear in simulated variations for the polarization ratio (PR). Comparisons with ground-based radiometric measurements show that the simulations based on snow SSA measurements have to be scaled with a model-specific factor of Do in order to minimize the root mean square error (RMSE) between measured and simulated T_B. Results using in-situ grain size measurements (SSA or D_{max}, depending on the model) give a mean T_B RMSE (19 and 37 GHz) of the order of 16–26 K, which is similar for all models when the snow microstructure metrics are scaled. However, the MEMLS model converges to better results when driven by the correlation length estimated from in-situ SSA measurements rather than D_{max} measurements. On a practical level, this paper shows that the SSA parameter, a snow property that is easy to retrieve in-situ, appears to be the most relevant parameter for characterizing snow microstructure, despite the need for a scaling factor.

© 2017 Elsevier Inc. All rights reserved.

1. Introduction

In snow remote sensing, a better parameterization of the radiative transfer models (RTM) for simulating snow microwave emission improves our ability to retrieve snowpack characteristics from spaceborne observations. Snow microstructure metrics are the main input parameter of the microwave RTM (e.g. Rutter et al., 2009) and its characterization can strongly impact the retrievals from microwave emission measurements for snow monitoring (e.g. Mätzler, 1994; Armstrong and Brodzik, 2002; Kelly et al., 2003; Mätzler et al., 2006; Löwe and Picard, 2015). Thus, given that the available models that are well-defined in the literature and commonly used for snow remote sensing are defined by different snow microstructure parameterizations, a review appears essential. We consider here the following four models: the Dense Media Radiative Transfer- Multi layers (DMRT-ML) model (Picard et al., 2013), the Dense Radiative Transfer Model - Quasi-Crystalline Approximation (QCA) Mie scattering of Sticky spheres (DMRT-QMS) model (Chang et al., 2014), the multi-layer Helsinki

* Corresponding author at: Centre d'Applications et de Recherches en Télédétection (CARTEL), Université de Sherbrooke, 2500 boul. Université, Sherbrooke, QC, Canada J1K 2R1.
E-mail address: Alain.royer@usherbrooke.ca (A. Royer).
[1] Now at the Canadian Ice Service, Environment and Climate Change Canada, Ottawa.

http://dx.doi.org/10.1016/j.rse.2016.12.020
0034-4257/© 2017 Elsevier Inc. All rights reserved.

University of Technology model (HUT-nlayers) (Lemmetyinen et al., 2010a), and the Microwave Emission Model of Layered Snowpacks (MEMLS) (Proksch et al., 2016; Wiesmann and Mätzler, 1999; Mätzler and Wiesmann, 1999). Several aspects of these models are based on different electromagnetic theories or semi-empirical approaches (multiple scattering and absorption coefficient computations, for example), and they are often driven by sets of different measured inputs for snow grain metrics, such as snow specific surface area (SSA), correlation length or snow grain geometrical extent obtained from visual analysis.

Tedesco and Kim (2006) compared earlier simplified single-layer versions of the DMRT, HUT and MEMLS models based on the snow grain metric given by visual inspection (average size over the snowpack depth of representative small, medium, and large grains in each layer measured using a microscope). MEMLS and HUT-nlayers were compared by Lemmetyinen et al. (2010b) and Pan et al. (2016). DMRT theory and IBA were also recently compared and analyzed (Löwe and Picard, 2015), while Roy et al. (2013) compared DMRT-ML and HUT-nlayers. Sandells et al. (2016) compared DMRT-ML, HUT-nlayers and MEMLS models considering only the optical diameter generated by snow models. But the four multi-layer models considered were never compared together using coincident sets of measured snow properties. The main challenge in comparing these RTM models is that the input snow microstructure parameters differ in each model and are in some cases difficult or impossible to measure in the field. Three different snow microstructure representations are considered in these models: optical diameter (D_o) and stickiness for DMRT-ML and -QMS, correlation length (p_c) for MEMLS and maximum geometrical extent (D_{max}) for HUT-nlayers. Consequently, some hypotheses are needed for their estimation allowing coherent intercomparison of models (Löwe and Picard, 2015). For example, it was previously shown that the optical diameter derived from the SSA needs to be scaled by a factor in order to be in agreement with measurements when considering DMRT-ML with non-sticky medium (Brucker et al. 2011; Roy et al., 2013; Montpetit et al., 2013; Picard et al. 2014; Dupont et al., 2014). As the physical aspects of each model had already been extensively analyzed, we put the emphasis in this paper on comparing the models with surface-based measured brightness temperature (T_B). The objective is to compare the simulations using the same in-situ measurements of improved snow parameterization, which had never been done.

This paper briefly recalls the main basic fundamentals of these four models and more specifically the different grain size definitions involved (Section 2). After presenting datasets and snow microstructure measurement methods (Section 3), we first compare the four models using a synthetic snowpack to perform a sensitivity analysis (Section 4.1), and we then compare the simulated T_B using sets of measured snow properties against measurements of surface-based radiometric T_B at 11, 19 and 37 GHz (Section 4.3).

2. Models and their respective snow microstructure metric

A synthesis matrix of the four models considered in this study is presented in Table 1. These models are all publicly available (thus specific details of their implementations can be known) and are extensively described in the references given in Table 1. Readers are invited to consult these references for detailed descriptions of the models, which are based on conceptually different approaches for computing snow electromagnetic properties and radiation transfer in the multi-layers of the snowpack. In this paper, all the simulations were performed using the recommended configuration for DMRT-ML and -QMS, the Improved Born Approximation (IBA) (option 12) for MEMLS and the original version of the extinction coefficient in HUT (see Table 1).

One of the main difficulties in snow radiative transfer is the parameterization of snow microstructure consisting of a high density of scatterers per unit of volume. DMRT-ML and -QMS consider the snow as a collection of sticky spherical ice particles defined by their radius and stickiness (Tsang and Kong, 2001; Tsang et al., 2007), while MEMLS parameterizes snow microstructural properties by a second order statistical function, the two-point correlation function, giving the mutual relationships between two scatterers within a given volume, such as the autocorrelation function (the exponential correlation length p_{ex} is generally used, see Section 2.2 below). HUT is based on empirical scattering and extinction coefficients fitted with the observed maximum dimension of snow grains (D_{max}), or more recently an effective grain size radius (Kontu and Pulliainen, 2010). When using in-situ ground-based measurements of snow microstructure parameterization, practical comparison of these models requires hypotheses to retrieve and link the different metrics. The metrics used in this study are briefly defined below.

2.1. DMRT snow microstructure metric

DMRT-ML considers snow grains as spherical particles of ice defined by their radius. Their position (clustering) is controlled by stickiness. For snow having a wide range of grain shape, the radius of equivalent spheres can be objectively defined by their optical radius (Ro), which can always be derived from the SSA via the optical equivalent radius. The snow SSA is the surface of the air/snow interface (S) per unit of mass: $M = \rho_{snow}$volume: $SSA = S/M = S/(\rho_{ice}\text{volume})$ in $m^2\ kg^{-1}$, where ρ_{ice} is the ice density (917 kg m^{-3}). SSA measurements are described in Section 3. For spheres or snow assimilated as sphere equivalent (see the review paper by Domine et al., 2008), the optical radius (Ro) is expressed as (Ro in mm, ρ_{ice} in kg m^{-3} and SSA in $m^2\ kg^{-1}$):

$$Ro = 3.10^3/(\rho_{ice}\ SSA) \quad (1)$$

Since any measurements can be used to estimate stickiness, Brucker et al. (2011), Roy et al. (2013), Dupont et al. (2014) and Picard et al. (2014), considering a non-sticky medium, have shown that Ro should be multiplied by the scaling factor ϕ_{DMRT} when Ro is derived from SSA measurements (R'o in mm):

$$R'o = \phi_{DMRT}Ro = 3.10^3\phi_{DMRT}/\rho_{ice}\ SSA \quad (2)$$

This scaling factor is discussed in Section 2.4. Roy et al. (2013) also showed that the following relationship (inspired by Kontu and Pulliainen, 2010) can be used for an effective optical radius of snow grains derived from SSA measurements:

$$R"o[mm] = 1.1\left[1 - \exp(-24.6.10^3/(\rho_{ice}\ SSA)\right] \quad (3)$$

The stickiness parameter (τ), used by DMRT theory (Tsang and Kong, 2001), is inversely proportional to the contact adhesion between spheres. It can be linked to the cohesion or to a degree of connectivity between grains. Thus, for non-sticky spheres: $\tau = \infty$; for snow with clusters (aggregates) or grains with high strength of adhesion, τ decreases (for example $\tau = 1$ to 0.2 or less). DMRT-ML uses the "short range" approximation (Tsang and Kong, 2001) which implies that grains and aggregates should remain small compared to the wavelength. Roy et al. (2013) hypothesized that the needed scaling factor (ϕ_{DMRT}) is related to the assumption of non-sticky spheres ($\tau = \infty$) and to the assumption of monodisperse grain size distribution. This scaling factor is therefore a surrogate of the stickiness parameter which cannot practically be measured in the field (see Löwe and Picard, 2015).

2.2. MEMLS snow microstructure metric

MEMLS uses the correlation length (p_c) for describing snow microstructure, which is the slope of the spatial autocorrelation function at the origin (i.e. the derivative of this function). This parameter might be derived from micro-computed tomography measurements (micro-CT) (Löwe et al., 2013) or by high-quality stereological method (see

Table 1
Comparison between basics of DMRT-ML/-QMS, MEMLS and HUT-nlayers models. See below for the definitions of terms.

Model	DMRT-ML		DMRT-QMS	MEMLS (V3)[a]		HUT-nlayers
Version	V1.6 (with several options)		V 0.1	IBA version	Empirical version	2015
Physical principle	Maxwell equations + several approximations considering a collection of densely packed sticky spheres			Empirical relationships between micro-structure and scatt/abso/ext. coefficients and empirical relation for the dependence of the polarization factors on volume fraction		
Theory	Dense Media Radiative Transfer Model (Shih et al. 1997) (Tsang et al., 2013)			Improved Born Approxi-mation (IBA)[b] (Mätzler,1998)	Empirical scattering coef. (Weismann et al., 1998)	Semi-empirical relation
Typical range of frequency	1–100 GHz					
Approxi-mations options	Recommended option • QCA-CP[c] • Rayleigh assumption • Optional correction for large particles (Grody, 2008) • Mono-disperse sphere radius • No stickiness • Optional stickiness • Optional bubbly ice	Research option • QCA-CP • Rayleigh assumption • No large particles • Poly- disperse (i.e. Rayleigh distribution) • No stickiness	Quasi-Crystalline Approximation (QCA) of Mie scattering • Optional stickiness	• Combination of coherent and incoherent (scattering) reflection between interface layers • Coherence effect for thin ice layer • IBA: option 12 • Ice without air bubble ($p_{ex} = 0$)	• Different scattering coef.: options 8,10,11	• Empirical scat. coef. • Semi-empirical absorption coef. $\kappa_e(1/m) = \alpha f^2 D_{eff}^{2.8f}$ $\kappa_e(1/m) = \beta(f^4 D_{eff}^6)^{0.2g}$ • Ice as high density snow with $R_{eff} = 0$
Snow micro-structure parametrization[d]	Spheres defined by their radius (Ro) and their stickiness (τ)			Correlation length (p_c or p_{ex}) for 5 to 100 GHz, the model is defined by the correlation length range from 0.05 up to 0.6 mm (Mätzler and Wiesmann, 1999)		Grain geometrical extent (D_{max}) Grain effective diameter ($D_{max,eff}$)
Liquid water content	Wetness fractional volume of water with respect to ice vol.		No	Volumetric liquid water content W: 0 to about 0.15		Snow moisture (up to several %)
Radiative transfer between layers	DISORT[e] (recommended 64 streams or more)		DISORT[e] by eigenvalue-quadrature analysis	2 or 6 streams		1 streams (empirical coef. for forward scatt $q = 0.96$)
	Fresnel reflection coef. for snow/snow and snow/atmosphere interfaces					
Main ref.	Picard et al. (2013) Brucker et al. (2011) Roy et al. (2013) Dupont et al. (2014)		Chang et al. (2014) Huang and Tsang (2012) Liang et al. (2008) Tsang et al. (2007)	Proksch et al. (2016) Mätzler and Wiesmann (2014) Wiesmann and Mätzler (1999) Mätzler and Wiesmann (1999) Wiesmann et al. (1998) Mätzler (1994, 1997, 1998, 2004) Schwank et al. (2014)		Lemmetyinen et al. (2010a) Pulliainen et al. (1999) Kontu and Pulliainen (2010)
Web site	Open source GPL license http://lgge.osug.fr/~picard/dmrtml/		http://web.eecs.umich.edu/~leutsang/Available%20Resources.html	http://www.iapmw.unibe.ch/research/projects/snowtools/memls.html		Upon request

[a] MEMLS Version 3 (2014) uses updated formulas for the dielectric constants of ice and water. An L-band version of MEMLS was used by Schwank et al. (2014), assuming a simplified one-layer snowpack.
[b] IBA: the Improved Born Approximation (IBA) (Mätzler, 1998) expresses the scattering coefficient in terms of the Fourier transform of the two-point correlation function.
[c] QCA: the quasi-crystalline approximation (QCA) consists of approximating the resolution of the multiple scattering calculation in a dense porous environment by regarding this medium as a roughly crystalline structure, implying assumptions on the position of two particles between them considered fixed. QCA-CP: QCA can be optionally improved by the so-called Coherent Potential (QCA-CP) (Tsang and Kong, 2001). The basic concept of the CP is to regard the medium near each scatterer as an effective medium with a uniform effective scattering function of aggregates, which implies that the function remains constant in space. The CP approximation thus makes it possible to solve the calculation of the coherent potential Green's operator for multiple scattering (and in the QCA context in our case) assumed as constant in space.
[d] See text for the snow microstructure parameterization of each model.
[e] The Discrete Ordinate Method (DISORT) is used to numerically solve the radiative transfer equation (Jin, 1994).
[f] Extinction coefficient κ_e: $\alpha = 0.000415$, relationship for 18–60 GHz, Hallikainen et al. (1987).
[g] Extinction coefficient κ_e: $\beta = 0.461$ Roy et al. (2004).

Riche et al., 2012), but its rapid derivation from field measurements is still difficult. Recently, Proksch et al. (2015) proposed a relationship between Snow-Micropen measurements and correlation length that has not yet been validated for microwave emission applications.

Here, we first estimate the correlation length from the equivalent sphere grain radius (Ro) as proposed by Mätzler (2002), following the Debye relationship:

$$p_c = 4/3\ \mathrm{Ro}(1-\nu) \tag{4}$$

where ν is the ice volume fraction: $\nu = \rho_{snow}/\rho_{ice}$.

While there is no experimental relationship between simultaneous measurements of p_c (from micro-CT measurements) and SSA measurements, Montpetit et al. (2013) showed that the following relationship gives optimized simulated T_B using MEMLS driven with SSA measurements (p'_c in mm, density in kg.m^{-3} and SSA in m^2 kg^{-1}):

$$p'_c[\mathrm{mm}] = 4.10^3 \phi_{MEMLS} 1-\nu/\rho_{ice}\ \mathrm{SSA} \tag{5}$$

where ϕ_{MEMLS} is a scaling factor and SSA is measured in-situ. Throughout this paper, grain size metrics (e.g. radius or pc, pex) will be expressed in mm.

If the autocorrelation function is approximated (fitted) by an exponential function of the form: exp.($-$x/p_{ex}), one can derive the exponential correlation length p_{ex}. According to the type of snow, p_{ex} is different from p_c (Krol and Löwe, 2016; Matzler, 2002). For microwave measurements, p_{ex} is generally preferred to p_c, and Mätzler (2002) found in general that $p_{ex} \approx 0.75 p_c$, giving from (1) and (4):

$$p_{ex}[\mathrm{mm}] \approx \mathrm{Ro}(1-\nu) = 3.10^3(1-\nu)/(\rho_{ice}\ \mathrm{SSA}) \tag{6}$$

On the other hand, previous studies from Mätzler (1997) have shown that p_c is closer to the minimum characteristic extent of the grain than related to the maximum geometrical particle extent. Mätzler (2002) gives a series of measurements of p_c, p_{ex} and visually estimated grain size D_{max} (defined below) for 20 samples of different snow types showing the correspondence between these parameters. Using these data, p_{ex} (or p_c) can be expressed as a logarithmic function of Dmax:

$$\begin{aligned} p_{ex} &= a + b\ \ln(D_{max}) \text{ for } \nu > \nu_{th} \text{ and } D_{max} > D_{max,th} \text{ in mm} \\ p_{ex} &= C^{st} \text{ otherwise} \end{aligned} \tag{7}$$

where ν_{th} and $D_{max,th}$ are thresholds delimitating the range of validity of the proposed model, and C^{st} is a constant for values below these thresholds.

Using the Mätzler (2002) data, Durand et al. (2008) found that a = 0.18 and b = 0.09 for $\nu > 0.2$ and $D_{max} > 0.125$ mm, and that $p_{ex} = 0.05 \pm 0.017$ mm otherwise.

2.3. HUT snow microstructure metric

HUT input is based on individual grain size. There are many ways to describe the geometrical grain size of snow (Colbeck et al., 1990; Lesaffre et al., 1997; Fierz et al., 2009). Among them, one can cite the circle (or ellipsoid) that better encompasses the snow grain; the equivalent radius given by the ratio between projected grain area and its perimeter; the mean convex radius of curvature; or the greatest extent of the prevailing or characteristic grains: Dmax. The latter corresponds to the maximum dimension of the "intermediate grain size" and has long been a classical parameter routinely used to visually characterize snow structure in the field (see Colbeck et al., 1990; Fierz et al., 2009). The HUT model can be driven either directly by D_{max}, or by an effective grain diameter ($D_{max,eff}$) derived from Dmax following the relationship that minimized the differences between measured and simulated T_B, as proposed by Kontu and Pulliainen (2010) (see also Lemmetyinen et al., 2010a, 2015; Pan et al., 2016):

$$D_{max,eff} = 1.5(1 - \exp(-1.5\ D_{max})) \tag{8}$$

where $D_{max,eff}$ and D_{max} are in mm.

However, in this study, it appears that this relationship (Eq. (8)) for estimating the $D_{max,eff}$ does not give a good agreement, due to the lack of convergence in the optimization. This results from the large digitized D_{max} measurement values obtained in this study (see Section 4.2), and Eq. (8) leads to a unique $D_{max,eff}$. In the model comparison (Section 4.3), we thus consider $D_{max,eff} = 0.5\ D_{max}$, derived from an optimization that reduces the difference between simulated and measured T_B (method of Roy et al., 2013).

When SSA is measured, Roy et al. (2013) use Eq. (2), with a different scaling factor (ϕ_{HUT}) relative to the effective grain size in HUT simulations:

$$Do_{eff}[\mathrm{mm}] = 6.10^3 \phi_{HUT}/(\rho_{ice}\ \mathrm{SSA}) \tag{9}$$

All the ϕ factors (ϕ_{DMRT}, ϕ_{MEMLS} and ϕ_{HUT}) are further discussed in Section 2.4. Field measurement methods for SSA and D_{max} estimates are presented in Section 3.

2.4. Scaling factors for the models driven by SSA measurements

The scaling factor ϕ depends upon the model considered and the type of snow. The change in this scaling factor is linked to other microstructure parameters such as stickiness and to the fact that we assume a monodisperse size distribution of snow grain (see the discussions in Brucker et al., 2011; Roy et al., 2013 and Löwe and Picard, 2015). It cannot be explained by measurement uncertainties (Roy et al., 2016). Löwe and Picard (2015) theoretically demonstrate the need of grain size scaling between the optical diameter and the equivalent sticky hard sphere diameter. For DMRT-ML with the assumption of non-sticky spheres, the ϕ factor obtained varies from 2.3 to 3.5 depending on the type of snow (Table 2). The amplitude of this factor may also partly be affected by errors in snow measurements and possibly in the soil parameters. Precise explanation of these differences in the ϕ factor needs further study but is outside the scope of this paper. Here we used $\phi = 3.3$, 1.3 and 3.7, respectively for DMRT-ML, MEMLS and HUT-nlayers (Table 2) in order to compare the known optimized models when driven by SSA measurements compared to simulations driven by D_{max} measurements.

2.5. Radiative transfer model inputs

Apart from the snow microstructure parameterization, all other input parameters required by the four models are the same for each layer defined by its thickness, snow temperature and density. Here, we only considered dry snow. An important contribution to snowpack emission can emanate from the soil under the snowpack, in particular at low frequencies. For the intercomparison in this study, we thus used the same rough soil reflectivity model proposed by Wegmüller and Mätzler (1999) (see the review of Montpetit et al., 2015a). At a given frequency, the soil parameterization is defined by the soil/snow interface reflectivity in horizontal polarization (Γ_H) and vertical polarization (Γ_V) with the following equations for an incidence angle (θ) lower than 60°:

$$\begin{aligned} \Gamma_H &= \Gamma_H^{Fresnel} \exp\left(-(k\sigma)^{\sqrt{-0.1cos\theta}}\right) \\ \Gamma_V &= \Gamma_H\ cos\theta^{\beta} \end{aligned} \tag{10}$$

where k is the incident medium wave number (air or snow), $\Gamma_H^{Fresnel}$ is the Fresnel reflectivity function which depends on the soil permittivity (ε_{soil}), σ is the soil roughness parameter and β is a scaling factor for deriving the reflectivity at vertical polarization from the computed

Table 2
Scaling factor ϕ to be applied on the snow microstructure metric derived from in-situ SSA measurements, as a function of the RTM considered and the type of snow. All SSA measurements were derived from the DUFISSS's type approach (see Section 3.1), except *: the values depend upon the method used for retrieving SSA; and **: SSA retrieved from ASSAP device (see details in the given references, last column).

Radiative transfer models	Snow μstructure metrics	Sites	ϕ	References
MEMLS	$p'_c = 4.10^3\,\phi(1-\nu)/(\rho_{ice}\,SSA)$ Eq. (5)	Canada: Arctic, Subarctic, South Québec	1.3	Montpetit et al. (2013)
DMRT-ML (no stickiness)	$R'o = 3.10^3\phi/(\rho_{ice}\,SSA)$ Eq. (2)	Dome C Antarctica	1.89, 2.5, 2.85*	Brucker et al. (2011)
		Dome C Antarctica	2.3**	Picard et al. (2014)
		Barnes Ice Cap Canada Arctic	3.5	Dupont et al. (2014)
		Canada: Arctic, Subarctic, South Québec	3.3	Roy et al. (2013)
HUT-nlayers	$Ro_{eff} = 3.10^3\phi/(\rho_{ice}\,SSA)$ Eq. (9)	Canada: Arctic, Subarctic, South Québec	3.7	Roy et al. (2013)

reflectivity at horizontal polarization. Following Montpetit et al. (2015b), we consider the optimized values of ε_{soil}^{eff}, σ^{eff} and β^{eff} parameters for each frequency given in Table 3.

For comparisons between simulated T_B and measurements, the downwelling sky radiance reflected by the snowpack toward the radiometer has to be taken into account (Montpetit et al., 2013; Courtemanche et al., 2015; Roy et al., 2016). In each surface-based radiometric measurement, the atmospheric contribution was calculated using the atmospheric Millimeter-wave Propagation Model (MPM: Liebe, 1989) implemented in the HUT snow emission model (Pulliainen et al., 1999). The atmospheric model was driven with the air temperature and precipitable water of the atmospheric layers above the surface given by the 29 atmospheric layers of the North American Regional Reanalysis (NARR) (Mesinger et al., 2006) for the NARR pixel and time of measurements. Note that all the snowpits were located in open areas where no vegetation could contribute to the measured T_B (see the discussion in Roy et al., 2016). We previously validated this procedure against sky microwave measurements (see Courtemanche et al., 2015).

3. Ground-based measurement dataset

3.1. Optical radius retrieved from SSA measurements using IRIS

A light short-wave infrared laser-based system measuring snow albedo through an integrating sphere (InfraRed Integrating Sphere, IRIS), similar to the system previously proposed by Gallet et al. (2009), was used for SSA measurements (Montpetit et al., 2012). Relatively good accuracy (12–15%) and reproducibility in SSA measurements are obtained using the IRIS system on extracted samples. Gallet et al. (2009) and Montpetit et al. (2012) describe in detail these devices (Dual Frequency Integrating Sphere for Snow SSA: DUFISSS and IRIS, respectively). Lambertian targets with known reflectance values (spectralon: 0.06, 0.25 0.60, 0.79, and 0.98 at 1.33 μm) were used to calibrate the device before and after each series of measurements at each site. From the reflectance, the SSA was calculated as described by Montpetit et al. (2012). SSA measurements allow us to estimate the mean optical radius of grain sizes of each layer (Eq.(1)), assuming that all grains have the same size (monodisperse size distribution).

3.2. D_{max} measurements using multidirectional lighting macrophotos in the shadow-box

Macrophotos of snow grain samples have been widely used in numerous studies (e.g. Colbeck, 1990; Fierz et al., 2009). In order to improve geometrical snow grain parameterization, we developed an optical system that uses, within an enclosed box (30 × 30 × 30 cm), five light-emitting diodes that provide five-direction (nadir, N, E, S and W) illumination of a gridded plate upon which snow grains are placed (Fig. 1). Five photographs are taken successively for each illuminated direction with a Nikon D40 fitted with a macro lens (Fig. 1). The projected area of the grain is extracted from a first photograph with the diode illuminating from nadir and the four other photographs allow the digitization of the projected shadows. Knowing the angles of illumination and the exact position of each grain on the gridded illuminated plate, it is possible to calculate the height of the grain envelope using the tangent illumination path corresponding to the projected shadow in each direction. We thus derived a numerical height model of each snow grain and reconstructed a 3D representation of the snow grain envelope (Fig. 1). From this elevation model, one can derive multiple size parameters: D_{max}, minor and major axis of the envelope ellipsoid, projected area, mean height, maximum height and apparent volume and surface area. All of these parameters are then averaged for each sample. This device (called shadow-box) is very easy to handle in the field, and improves the retrieval of a 3D representation of the snow grains. It is also useful to characterize snow grain shapes and types of extracted snow samples. Using calibrated spheres (steel balls from 0.8 to 4.8 mm), the retrieval error (bias) on D_{max} was estimated of the order of 0.03 mm. The measurement protocol is as follows: we gently cover the plate with separated grains of a snow sample extracted from each snowpack layer (approximately every 3 cm over the snowpit), and take the five consecutive macrophotos, including identifications of the snowpit and layer. We then systematically manually digitize the contour of all the grains on the plate to estimate the mean D_{max} (2D) values for each snowpack layer. The shadows help to discriminate individual grains in aggregates or when grains are stuck together.

Table 3
Soil parameters considered for the three models (see Eq. (10)).

Frequency (GHz)	ε_{soil}^{eff}	β^{eff}	σ^{eff} (cm)
11	3.18–0.006134j	1.08	0.19
19	3.42–0.00508j	0.72	
37	4.47–0.32643j	0.42	

3.3. Correlation length

Since no direct measurement of correlation length was carried out, the values of correlation length (p_c or p_{ex}) used as inputs for MEMLS were estimated in three ways: (1) from the retrieved optical grain size radius (SSA measurements) and the fractional volume (Debye relationship, Eq. (5)) (hereafter labeled MEMLS_Do); (2) from the measured values of mean D_{max} grain size (2D shadow-box) and fractional volume based on the Mätzler relationship (Durand et al., 2008) (hereafter labeled MEMLS_D_{max_pex}); and (3) from p_{ex} based on the observed linear relationship between p_c and Dmax shown in the results section (see Fig. 5) (hereafter labeled MEMLS_D_{max}_lin).

3.4. T_B measurements

All the measurements analyzed in this paper are those already used before and are described in references given in Table 4. T_B measurements were taken for every snowpit at 10.67 (hereafter noted 11), 19 and 37 GHz in vertical polarization (V-pol) and horizontal polarization (H-pol) at a height of approximately 2 m above the surface using PR-series field radiometers (Radiometrics Corporation, Boulder, CO, USA) at

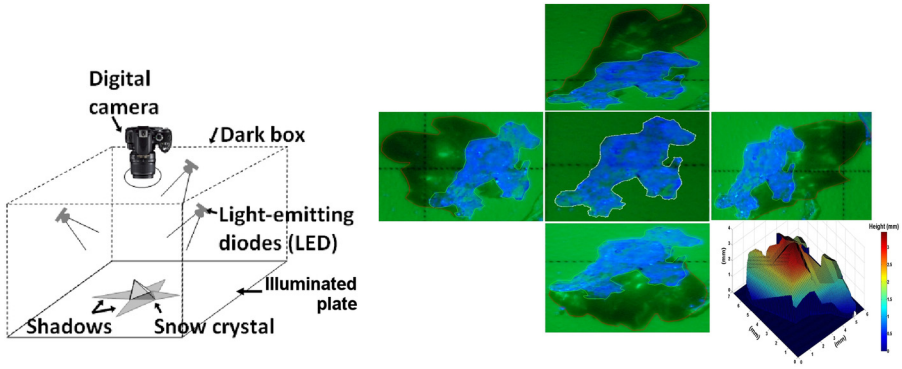

Fig. 1. Shadow-box. Snow grains placed on the plate are successively illuminated from four directions by four LEDs and by one LED from the nadir, producing five macrophotos (right), from which a 3D envelope model of the grain can be retrieved after manual digitization of the shadows. The size of the grain shown is 7 mm.

an incidence angle of 54°–55°, which is close to the measurement incidence angle of the Advanced Microwave Scanning Radiometer - Earth Observing System (AMSR-E) and Special Sensor Microwave Imager (SSM/I) space-based sensors. The ellipsoidal footprint of measurements at the snow surface was approximately 0.5 m × 0.65 m. The radiometer calibration was based on two measurements taken with the absorbing foam Eccosorb© (Cuming Microwave Corporation, MA, USA) at the ambient temperature (i.e. warm reference) and another taken over a surface of liquid nitrogen (i.e. cold reference) (Asmus and Grant, 1999; Langlois, 2015). In the worst case, measurement error for the calibration target was estimated at ±2 K. Ambient and cold point measurements from before and after the field campaign periods (typically separated by five to ten days) were used to produce a final calibrated T_B data set.

Table 4
Summary of the snow parameters of all sites analyzed in this study. Site name: CHxx corresponds to Churchill, MB sites (Roy et al., 2013; Montpetit et al., 2013); SIRSP4 and RoSP1 correspond to the southern Québec sites, respectively to the SIRENE site at Sherbrooke, QC and to the St-Romain, QC site (Roy et al., 2013); BJxx sites corresponds to the James Bay, Nunavik, QC sites (subarctic sites) (Roy et al., 2016). The snowpits where an ice lens was observed are identified (last column).

	Site name	Snow depth (m)	Tsnow (K)	Density (kg/m^3)	Tsoil (K)	Optical radius (mm)	Dmax (mm)	Bulk p'$_c$ (Eq. (5))	Ice lens
1	CH42	0.37	259.4	289.4	267.9	0.22	4.43	0.267	
2	CH43	0.70	257.3	311.4	270.3	0.20	2.68	0.231	
3	CH83	1.18	269.4	372.6	272.7	0.19	2.83	0.199	
4	CH90	0.82	265.3	284.0	271.8	0.18	3.43	0.213	
5	CH91	0.91	267.1	324.7	272.5	0.19	4.16	0.210	
6	CH92	0.83	268.3	292.8	272.9	0.22	3.10	0.262	
7	CH95	1.74	266.0	380.3	272.8	0.15	1.89	0.150	
8	CH96	1.80	266.8	367.8	272.9	0.17	2.20	0.172	
9	CH97	1.50	266.4	380.9	272.7	0.18	2.07	0.178	
10	CH98	1.19	265.8	351.4	272.5	0.16	2.04	0.166	
11	CH104	0.48	255.2	261.4	269.6	0.32	4.90	0.393	
12	CH105	0.45	258.7	229.7	270.3	0.32	6.11	0.419	
13	CH111	0.44	252.5	284.6	269.8	0.25	4.54	0.303	
14	CH55	0.51	258.5	308.4	269.7	0.19	3.54	0.214	
15	CH56	0.35	254.9	314.6	267.2	0.20	3.15	0.231	
16	CH99	0.57	259.3	328.0	270.1	0.23	4.02	0.255	
17	CH101	0.19	259.1	263.2	264.6	0.33	4.88	0.403	
18	CH54	0.48	257.1	345.0	269.5	0.20	4.51	0.215	x
19	CH57	0.25	260.2	321.9	266.1	0.20	3.50	0.224	
20	CH58	0.35	256.5	304.6	267.9	0.16	4.84	0.189	x
21	CH59	0.65	260.2	276.6	271.7	0.23	3.71	0.274	x
22	CH60	0.14	270.4	288.3	262.2	0.27	3.83	0.325	x
23	CH61	1.03	260.5	400.8	272.5	0.19	2.68	0.187	
24	CH82	0.35	266.5	285.4	270.8	0.37	4.08	0.446	
25	CH93	0.82	279.6	311.9	271.9	0.28	4.43	0.325	x
26	CH100	0.43	259.8	295.8	269.2	0.28	4.78	0.328	x
27	CH114	0.72	283.2	323.0	272.8	0.33	3.19	0.373	x
28	CH115	0.31	271.4	313.6	272.2	0.33	5.11	0.382	
29	SIRSP4	0.33	271.5	245.9	273.0	0.14	3.07	0.173	
30	RoSP1	0.47	269.4	179.2	273.5	0.08	1.05	0.107	x
31	BJjan1	0.51	266.8	284.9	271.5	0.16	3.07	0.191	x
32	BJfev2	0.66	265.8	245.1	273.1	0.18	2.01	0.229	x

3.5. In-situ snow data

The snow data needed by the models were derived from in-situ measurements in three northern Canadian regions. Table 4 provides the data from the Arctic: Churchill (MB), the Subarctic region: James Bay (QC), and southern regions of Québec: Sherbrooke (QC) and St-Romain (QC). All sites were already well-described in the references given in the Table 4. This database of 32 snowpits encompasses a wide range of snow types (i.e. metamorphic processes and stratigraphy), typical of North American environments. For each site, profiles of snow temperature, snow density, and snow microstructure were taken at a vertical resolution of 3 or 5 cm in the footprint of the microwave radiometers. The density was measured with a 185 cm^3 density cutter, and the samples were weighed with a 100 g Pesola light series scale with an accuracy value of 1 g. The temperature was measured with a Traceable 2000 digital temperature probe (±0.1 °C). The microstructure of each layer was defined with both SSA (optical radius) and D_{max} measurements, the latter using macrophotos (Shadow-box). In Table 4, we give the vertically averaged values of density, optical radius and D_{max}, weighted by the snow layer thicknesses and the derived bulk p'$_c$ (from Eq. (5)) were also estimated (9th column). The stratigraphy was examined at each site, and all ice lenses (or crusts), when present, were identified and measured. Their density was not measured as this is very difficult to properly sample. All the microwave and snow measurements were always synchronised in time. All these 32 sites (Table 4) were used for model comparison.

4. Results

A sensitivity analysis is first performed to compare the four models considered with the same inputs considering a synthetic snowpack (Section 4.1). We then discuss the consistency between the grain size measurements (Section 4.2), and we compare the simulations with ground-based measurements (Section 4.3).

4.1. Sensitivity analysis of the three models

Based on an identical synthetic snowpack, we seek to illustrate model sensitivity to three parameters: grain size (Fig. 2); density (Fig. 3); and ice lens in the snowpack (Fig. 4).

Fig. 2 shows the comparison between the 37 GHz brightness temperature variations as a function of Do, using the four models in a very simple synthetic case defined by one layer of 1 m thickness with a mean uniform density of 250 kg m^{-3}. The incidence angle of T_B simulations is 55°. All input parameters were the same for the four models and the different microstructure metrics were derived from the same initial

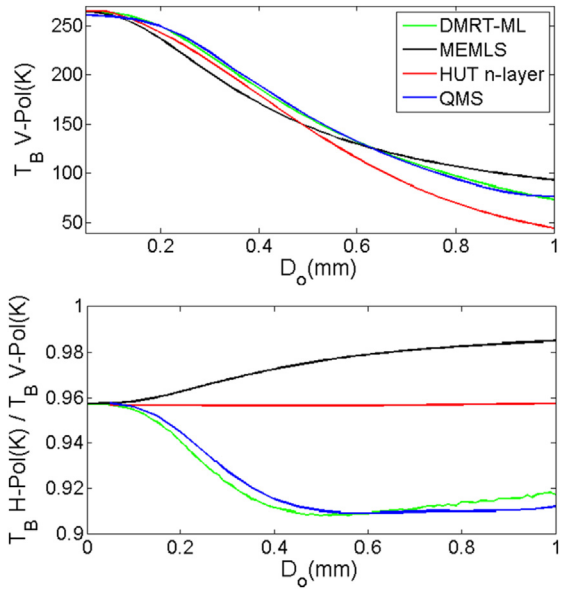

Fig. 2. T_B variation at 37 GHz as a function of the optical diameter (Do) of grain size for the four models. Top: T_B at the vertical polarization; bottom: polarization ratio (H-pol/V-pol). Simulations performed using Eq. (11) for the snow grain size definitions and the Wegmüller and Mätzler (1999) soil model (Table 1); soil temperature = 273 K; soil roughness = 0.19 cm, dielectric permittivity = 4.53 and the polarization reflectivity factor beta = 1.1 (Montpetit et al., 2015a); snow density = 250 kg m^{-3}; snow depth = 1 m; snow temperature = 263 K; no stickiness and no ice lens. The incidence angle of T_B simulations is 55°.

grain parameter (Do) using Eqs. (2), (5) and (9). To define the optical diameter of each model, we used the scaled factors defined in previous analysis (see discussion in Section 4.2). These factors optimize the simulations compared to in-situ radiometric measurements for real snowpacks. The relationships defining the microstructure metrics were derived from Eqs. (2), (5) and (9), respectively for DMRT-ML (assuming non-sticky spheres) (Roy et al., 2013), MEMLS-IBA (Montpetit et al., 2013) and HUT (Roy et al., 2013). For DMRT-QMS, we used the same

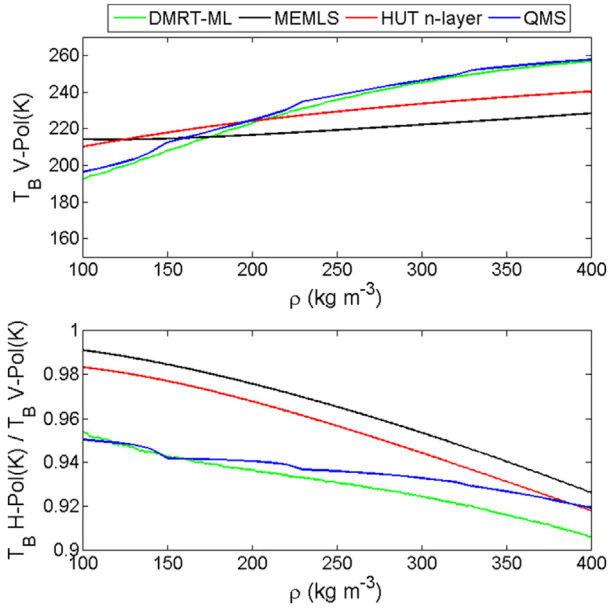

Fig. 3. Same as Fig. 2, but for density (Do = 0.25 mm).

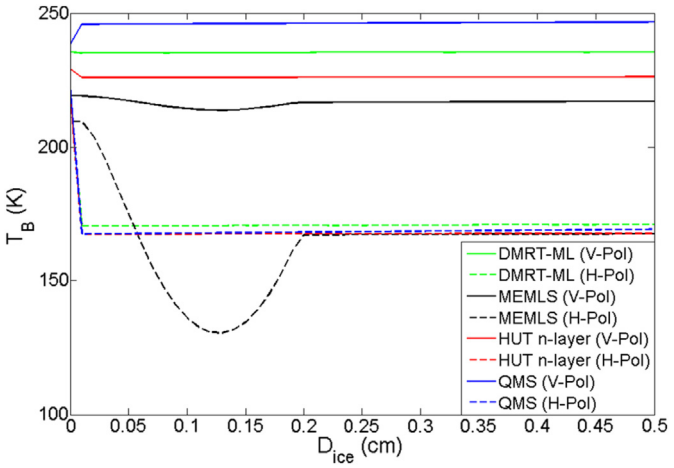

Fig. 4. T_B variation at 37 GHz as a function of an ice layer thickness (D_{ice}) put on the top of the snowpack for the four models (full lines: V-pol; dotted lines: H-pol). Snowpack and soil properties are the same as in Figs. 2 and 3 (Do = 0.25 mm and density = 250 kg m^{-3}). Ice lens density = 917 kg m^{-3} and ice lens temperature is the same as snow temperature.

relationship as for DMRT-ML, and also assuming non-sticky spheres. The comparison in Fig. 2 is thus performed using the following equations:

$$\begin{cases} \text{DMRT-ML/-QMS} : D'o = 3.3\ \text{Do} \\ \text{MEMLS} : \ p'_c = 1.3\ (2/3)\ \text{Do}\ (1-\nu) \\ \text{HUT} : \text{Do}_{\text{eff}} = 3.7\ \text{Do} \end{cases} \quad (11)$$

The results show that the T_B simulated by the four models similarly decrease with the grain size, as expected due to the high sensitivity of microwave attenuation to grain size at 37 GHz. Using the scaling factors for the input grain size metrics given in Eq. (11), the simulated T_B V-pol are close for Do around 0.5 mm and for Do < 0.2 (Fig. 2, top). However, MEMLS T_B values appear underestimated by 18 K compared to DMRT-ML/-QMS around Do = 0.3 mm. Note that DMRT-ML is identical to DMRT-QMS over the whole analyzed range of Do, as we stay in the Rayleigh range (see Picard et al., 2013), and despite the different formulation of the scattering coefficient. When the grain size becomes larger (Do > 0.6 mm, SSA < 11 m^2 kg^{-1}), the HUT-nlayers T_B significantly decreases, because this model empirically considers multiple scattering and is based on the 1-flux RT simplification, leading to underestimate downward-propagated T_B and then upward reflected and backscattered signal. Multiple scattering increasing with grain size tends to increase the upward radiation, compensating for the T_B attenuation.

The main polarization effects arise from reflections at layer interfaces, and are at their maximum near the Brewster angle (around 55° at 37 GHz), leading to a significant decrease of the T_B (H-pol) with incidence angle, while T_B V-pol is weakly independent of the incidence angle. Fig. 2 (bottom) shows the Polarization Ratio (PR = T_B H-pol/T_B V-pol) variations for the four models as a function of the optical grain size simulated for a fixed incidence angle of 55°. DMRT-ML and DMRT-QMS are also identical in this case. The HUT model practically neglects the scattering polarization variations with growing grain size, while DMRT-ML/-QMS and MEMLS models show different trends in PR variations with grain size. The MEMLS volume scattering in snow is slightly sensitive to polarization (Wiesmann et al., 1998) with a weak PR increase of 2% when the grain size increases between Do = 0.1 to 0.6 mm, while DMRT-ML/-QMS decreases by 4%, leading to a difference of about 7% compared to MEMLS for grain sizes above 0.6 mm (Fig. 2, bottom).

For a given fixed density, the polarization is modulated by 2 mechanisms: snow scattering and interface reflection. As snow-air interface reflections are similarly treated in each model (assuming Fresnel's

reflection) and because the density remains constant in these simulations, the differences between the three types of models (DMRT-ML/-QMS; HUT-nlayers and MEMLS) result from the differences in the radiative transfer solution. As a matter of fact, polarization effects are generated by volume scattering driven by the granular structure of the medium, i.e. by a combined effect of snow grain size and density (see Mätzler, 1997) and also of stickiness for DMRT-ML/-QMS (see Picard et al., 2013). The observed differences in PR variations in Fig. 2 (bottom) could thus likely governed by differences between the radiative transfer processing of the diffuse scattering component of the signal. The results for lower incidence angles (i.e. not Brewster) are similar.

We performed simulations (not shown) using a new model (in progress, unpublished) using the same N-flux solver used in DMRT-ML but which can compute scattering coefficients with either the DMRT theory (as in DMRT-ML and DMRT-QMS) or IBA (as in MEMLS). In both cases, assuming the same scattering theory, the results show a decrease of the PR with increasing Do, while the MEMLS-IBA (6-flux) shows an increase of the PR. This suggests that the radiative transfer processing, specifically 6-flux versus N-flux, could be the cause of the different behaviors observed in Fig. 2 (bottom), but further exploration of the role of the solver is needed.

The patterns of T_B variation with snow density show similar behaviors between models but at different amplitudes (Fig. 3). Here, Do is considered constant and equal to 0.25 mm. Over the range of density variation shown, below 400 kg m^{-3} (i.e. below 44% fractional volume), at vertical polarization, DMRT-ML/-QMS shows a greater sensitivity, ΔT_B V-pol of 40 K for density from 150 to 300 kg m^{-3}, than MEMLS and HUT which vary slightly. For low snow density between 150 and 200 kg m^{-3} the four models are similar, but at a high snow density of 400 kg m^{-3}, the T_B(V-pol) difference between DMRT-ML/-QMS and MEMLS is 28.5 K. (and 21.3 K at H polarization) (Fig. 3, top). For coarser grain size (not shown), the differences in T_B V-pol versus density variations between models are amplified, due to the difference in scattering processing in each model.

PR variations in relation to density show parallel trends (Fig. 3, bottom), but the decrease in PR when density increases shows significant differences in slope values for each model (>2% difference at low density for MEMLS and HUT compared to both DMRT models). For high densities (near 400 kg m^{-3}), this decrease is greater with DMRT-ML than DMRT-QMS.

T_B H-pol varies as a function of density change between interface layers, mainly from reflection at the snow-air interface, and of snow scattering (grain size). Since Fresnel reflection is considered here, surface reflection depends on the snow dielectric constant and thus the density. Assuming a constant grain size (as in Fig. 3), as density increases, the reflection coefficient increases and T_B H-pol decreases, leading to the decrease in PR (as T_B V-pol is relatively constant at the Brewster angle). In other words, where snowpack evolution features slow metamorphism as is observed in Antarctica, PR clearly decreases with density. This was shown by Picard et al. (2014) from surface-based measurements at Dome Concordia (East Antarctica). Champollion et al. (2013) also showed that the observed 2000–2010 AMSR-E PR increase was in agreement with the observed decreasing surface snow density, also at Dome Concordia.

However, when the snowpack evolves during the winter through various metamorphic processes (increasing grain size), increasing layering (alternation of high- and low-density layers) and increasing density processes, PR direction changes over time appear less clear. Moreover, the surface roughness would produce a more diffuse scattering distribution, leading to weaker polarization, while ice layers or wind-slab snow crusts lead to a significant degree of polarization (e.g. Mätzler, 1994; Grenfell and Putkonen, 2008; Dolant et al., 2016). In general, since surface density and state are the most important characteristics influencing polarization, one expects a decrease in PR with time from snowfall. The DMRT simulations showed a PR decrease for both increasing grain size and density processes in the synthetic cases considered here (Figs. 2 and 3), while MEMLS and HUT show a PR decrease only as a function of increasing density.

The third sensitivity analysis (Fig. 4) shows the effect of a thin ice layer put at the top of the snowpack for the four models. At V-pol, there are almost no T_B variations due to ice lens while TB H-pol is reduced by up to 65 K when an ice lens is introduced. The stronger decrease in H-pol (ice lens vs. no ice) compared to the one at V-pol comes from the higher sensitivity to layer interface reflectivity at H-pol. Note that, in Fig. 4, the differences in TB V-pol amplitudes between models result from the configuration (Do and density) used for the simulations (see Figs. 2 and 3). Moreover, ice layer thickness variations have no impact on T_B variation, except when using the MEMLS model for thin ice layers. Around $D_{ice} = 0.125$ mm, MEMLS is as much as 43 K lower at H-pol than the DMRT and HUT models. This significant T_B decrease simulated by MEMLS for H polarization that appears for ice thickness under $\lambda/2$ is due to the coherent reflection that dominates the microwave behavior for layers of the size $\lambda/4$ (Weismann and Mätzler, 1999). The DMRT-ML and HUT-nlayers models do not take into account this attenuation effect of the quarter-wavelength resonance. In practice, as the ice layer thickness spatially varies in the footprint of the sensor (Rutter et al., 2014), such effects are generally less pronounced than in simulations, but can be clearly observed for thin ice lenses on or in the snowpack (see Montpetit et al., 2013; Roy et al., 2016).

4.2. Snow grain database comparison analysis

We analyzed 159 photographed plates from the 32 studied snowpits, corresponding to a total of 36,384 digitized grains with an average of 229 grains per plate. For each plate, we considered the mean maximum dimension of all the grains on the plate (D_{max}). For each corresponding layer, we also measured the snow SSA and density. It is well known that the relationship between Do and D_{max} is not one-to-one (see Langlois et al., 2010; Leppänen et al., 2015). However, in order to evaluate the consistency of the datasets, Fig. 5 shows the relationship between the calculated correlation length derived from SSA and density measurements (Eq. (5), $\phi = 1$) and the corresponding mean D_{max} for all the samples. The results show that this relationship appears somewhat scattered as expected, and more linear rather than the logarithmic relationship suggested by Mätzler (2002). But note that, for the latter case (for 20 samples), D_{max} values were visually determined, whereas, in our case, D_{max} were derived from digitized contours. The digitization, the very large number of data and also the computation of the mean values (over hundreds of grains) could explain that our D_{max} values are different than those visually determined. The digitization of grain size is considered as a more reproducible and more precise approach.

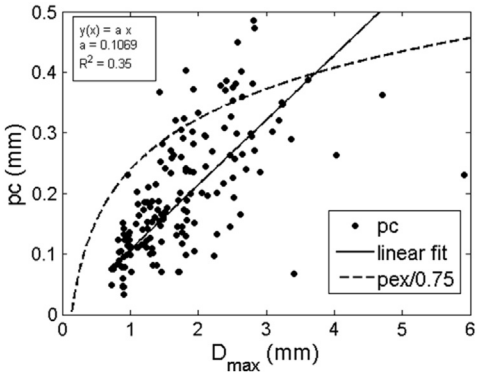

Fig. 5. Relationship between the correlation length derived from SSA and density measurements (p_c, calculated with Eq. 5, $\phi = 1$) and the mean maximum geometrical extent of the grains (D_{max}) measured by digitized photographs of snow grains (each point of this graph corresponds in average to 229 digitized grains per sample). The dotted curve corresponds to the logarithmic relationship observed by Mätzler (2002).

We also considered (not shown) median values instead of arithmetic means that did not give significant differences. On the other hand, the correlation lengths in the Mätzler (2002) database were measured (micro-CT) whereas we derived this parameter from SSA and density measurements. The reason for the differences between these microstructure metrics (D_{max}, SSA, correlation length), discussed for example by Löwe and Picard (2015), and which may also result from differences in snow types (alpine, boreal, arctic), is beyond the scope of this paper. This unique database (coincident values of Do, pc and D_{max}) was used to provide specific inputs to drive each model considered in order to simulate the brightness temperatures.

4.3. Model comparison using measured inputs

As DMRT-QMS is very similar to DMRT-ML, only three models are considered in the following: DMRT-ML, HUT-nlayers and MEMLS. For all the sites described in the Table 4, Fig. 6 compares the 3 model simulations against surface-based measured brightness temperatures with exactly the same soil parameters (Table 3), and for the snow microstructure metrics derived either from SSA or D_{max} measurements. DMRT-ML (Fig. 6a), HUT_Do (Fig. 6b) and MEMLS_Do (Fig. 6c) were driven by the scaled optical diameter of snow grain derived from SSA measurements. The HUT_D_{max} simulations (Fig. 6d) were driven by

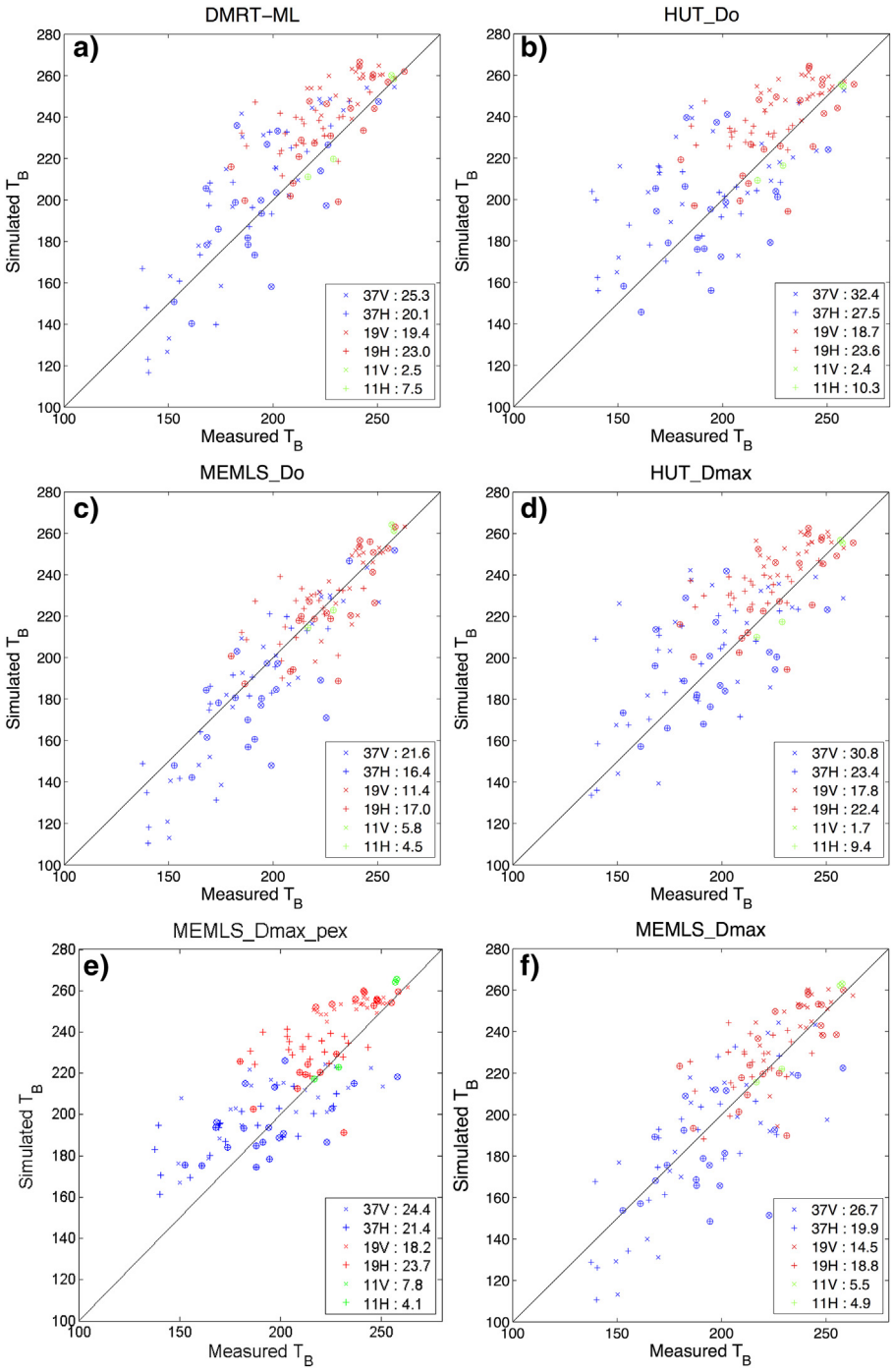

Fig. 6. Scatterplot comparing simulated brightness temperatures against measurements for each frequency and polarization for all the sites (described in Table 4). Circled symbols represent sites that included ice lenses. a: DMRT, b: HUT_Do (right); c: MEMLS_Do; d: HUT_Dmax; e: MEMLS_Dmax_p_{ex}; f: MEMLS_Dmax_lin. Input parameters are listed in Table 5. Values given in the figures correspond to the RMSE in Kelvin (reported in Table 6).

D_{max} measurements using an optimized scaling factor (see Section 2). Using D_{max} measurements, two inputs were also considered for MEMLS simulations: 1) MEMLS_D_{max}_p_{ex} (Fig. 6e) based on the Mätzler relationship (Durand et al., 2008, Eq. (7), see Fig. 5); and 2) MEMLS_Dmax_lin (Fig. 6f) based on the correlation length estimated by the observed linear relationship shown in Fig. 5. These model inputs are summarized in Table 5.

The root mean square errors (RMSE) and the biases are compared in Table 6 and shown in Fig. 7 for the three frequencies (11, 19 and 37 GHz) and each polarization. Note that the full set of input snow properties and 11 GHz radiometer measurements are only available for two sites, hence, the analysis focuses on 19 and 37 GHz.

For the 32 analyzed snowpits, the overall results at 19 and 37 GHz for the 6 model configurations show mean bias values of the order of 6 K, ranging from −10.8 to 16 K depending on the model, configuration and frequency considered. The mean RMSE value is of the order of 20 K (19 GHz) and 24 K (37 GHz), ranging from 11.4 to 32.4 K. Large differences in bias appear between models (MEMLS with negative biases), and no significant differences in bias or RMSE can be seen between polarizations. Note that except for HUT_Dmax (0.5 • Dmax), the models were not specifically optimized for the new cases considered in this study, since the used scaling factors were derived from previous publications over different sites.

MEMLS_Do seems to give slightly better results (mean RMSE of 14 K and 19 K, respectively at 19 and 37 GHz, for both polarizations) relative to other configurations and models (Figs. 6, 7, and Table 6). DMRT-ML results show a mean RMSE of 21 K (19 GHz) and 23 K (37 GHz) in this study, although we obtained better results for 45 other Arctic and Subarctic snowpits with the same parameterization (mean RMSE of 10 K (19 GHz) and 12 K (at 37 GHz), see Roy et al., 2016). The HUT model shows a lesser agreement at 37 GHz (mean RMSE of 30 K and 27 K respectively for the Do and D_{max} configuration).

MEMLS tends to underestimate the T_B at 37 GHz V-pol (negative bias), while the other models tend to overestimate the simulated T_B (positive bias). This is in accordance with the comparison using synthetic snowpacks (see Fig. 2, top), showing lower MEMLS T_B compared to DMRT and HUT for a large range of grain sizes.

Among the three analyzed MEMLS versions, it appears that MEMLS_Do performs best, compared to the D_{max}-based simulations (an average RMSE at 19 and 37 GHz of 16.6 K, 20 K and 22 K for respectively the MEMLS_Do, _D_{max}_lin and _D_{max}_p_{ex} configurations). As expected, the HUT model provides a slightly lower RMSE when using D_{max} (23.6 K) compared to HUT_Do (26.5 K). Moreover, at 37 GHz, DMRT using SSA appears better than the HUT model based on D_{max}. This confirms that the scaled SSA parameter is, in general, clearly better than the D_{max} parameter for describing snow grain size for microwave radiometry no matter the MEMLS or DMRT-ML model.

We showed (Fig. 4) that, for the synthetic snowpack, ice lens thickness within the snowpack could lead to significant differences in T_B among the models. Here, we accounted for the ice layer effects when they were observed in the snowpack, and the comparison shown in Fig. 6 does not exhibit systematic differences between snowpits with ice layers (10 sites/32, see Table 4) and those without ice layers. This first shows that ice layers can be adequately corrected for when their presence and particularly their position within the snowpit is known (see Montpetit et al., 2013; Roy et al., 2016), and secondly that ice layers cannot explain the differences in RMSE between models.

In terms of linear regression between simulated and measured T_B (coefficient of determination R^2 and slope of the regression), the model comparison (Table 7) also highlights the differences between models and configurations. Best results are obtained with DMRT-ML and MEMLS_Do, with a mean R^2 of the order of 0.75–0.79 for the 4 channels (T_B at 19 and 37 GHz and both polarizations). Results for these models are better at 37 GHz and with a slope slightly >1, meaning that the models underestimate low T_B values at this frequency (T_B < ~170 K). Even if MEMLS_Dmax_lin is really better than MEMLS_Dmax_p_{ex} for both R^2 and slope parameters, MEMLS_Dmax_lin performs less well than MEMLS based on Do. The HUT model gives here the worst agreement against measurements. Note that, in all cases (Table 7), the T_B H-pol values at 19 GHz show the lowest correlations, likely due to non-optimized processing of stratification between the snow layer interfaces, assumed specular, and for the soil-snow interface (roughness, for example). The statistics at 11 GHz are not included because there are only 2 measurements, but are included in the overall linear regression.

At last, we compared the simulated Polarization Ratio (PR H/V) at 37 GHz to the measured PR. The results show similar performance between the models (mean RMSE of 0.055). Also, we cannot conclude about the effect of the grain size on the PR trend (as simulated in Fig. 2). This relates to the fact that the sites integrate a large range of density and Do values, while Fig. 2 assumes a constant density when Do varies.

5. Discussion and conclusion

Over a large set of Arctic, Subarctic and boreal snow datasets, we derived a unique comprehensive snow grain size metrics database. These metrics were defined, on the one hand, by their specific surface area (SSA, from IR reflectometry measurements), and, on the other hand, for the same snow samples, by their mean maximum geometrical extent, called D_{max}, obtained from digitized macrophotos of snow samples at each layer. Here, we did not estimate D_{max} size by visual inspection as is generally done, because of the subjectivity of that approach. The digitization of each snow grain distributed on a photographed plate is thought to be a more robust and objective approach. This dataset allowed us to compare ground-based measurements of brightness temperatures (T_B) to the simulated T_B using four models driven by their specific metrics: DMRT-ML and -QMS with the optical diameter (Do) derived from SSA measurements; the HUT model with D_{max}; and the MEMLS model driven by the correlation length which can be estimated using both parameters (Do and D_{max}). We also tested the HUT model with Do, and we compared MEMLS simulations based on 2 different relationships for correlation length estimation. A total of six model configurations (Table 5) were thus analyzed (Figs. 6, 7, and Table 6).

Whatever the model considered, the scatterplots between simulated and measured T_B show somewhat large scatters (Fig. 6) due to the inherent uncertainties on all the parameters that affect the emitted signal, i.e. soil (temperature, dielectric permittivity and roughness), snow density stratification, snow temperature profile and snow grain size stratification (Roy et al., 2016; Durand et al., 2008). The obtained root mean square error between simulated and measured T_B are in the same

Table 5
Summary of the inputs used for the model simulations. The corresponding equations (Eq.) are explained in Section 2.

Model configuration	Grain size measurements	Input parameters	Eq.	Fig.
DMRT-ML	SSA	$D'o = 6.10^3\ 3.3/(\rho_{ice}SSA)$	2	6a
MEMLS_Do	SSA	$p'_c = 4.10^3\ 1.3(1-\nu)/(\rho_{ice}SSA)$	6	6c
MEMLS_D_{max}_p_{ex}	D_{max}	$-p_{ex} = 0.18 + 0.09\ \ln(D_{max})$ for $\nu > 0.2$ and $D_{max} > 0.125$ mm $-p_{ex} = 0.05 \pm 0.017$ otherwise	7	6e
MEMLS_D_{max}_lin	D_{max}	$p_c = 0.1069$ Dmax	Fig. 5	6f
HUT_Do	SSA	$Do_{eff} = 6.10^3\ 3.7/(\rho_{ice}SSA)$	9	6b
HUT_D_{max}	D_{max}	$D_{max,eff} = 0.5\ D_{max}$	–	6d

Table 6
Bias (B) and RMSE (R) (K) between simulated and measured T_Bs for each frequency and polarization and for each model driven by specific inputs (described in Table 5). Bold: minimum bias and RMSE values of each line respectively (but not necessarily statistically significant).

Model	**DMRT-ML**		**MEMLS**						**HUT**			
Inputs	Do $\phi = 3.3$		Do $\phi = 1.3$		D_{max}_lin (Fig. 5)		D_{max}_p_{ex} Eq. (7)		Do $\phi = 3.7$		D_{max} $\phi = 0.5$	
	B	R	B	R	B	R	B	R	B	R	B	R
11V	2.1	2.5	5.5	5.8	5.5	5.5	7.8	7.8	−2.1	2.4	**−1.1**	**1.7**
11H	−7.3	7.5	−4.1	4.5	−3.9	4.9	**−2.6**	**4.1**	−10.0	10.3	−9.1	9.4
19V	16.0	19.4	**0.1**	**11.4**	6.2	14.5	15.0	18.2	13.8	18.7	13.6	17.8
19H	14.7	23.0	**2.9**	**17.0**	7.8	18.8	15.0	23.7	8.5	27.5	13.4	22.4
37V	11.0	25.3	−10.8	**21.6**	−10.8	26.7	−10.8	24.4	11.3	32.4	**9.6**	30.8
37H	7.5	20.1	−4.9	**16.4**	**−3.3**	19.9	9.0	21.4	8.5	27.5	6.7	23.4
All	7.3	16.3	−3.1	12.8	0.3	15.0	5.6	16.6	5.9	19.1	5.5	17.6

range of values shown in previous studies that considered the same models (Roy et al., 2016; Pan et al., 2016; Löwe and Picard, 2015; Roy et al., 2013; Lemmetyinen et al., 2010b). The results analyzed here are thus representative of errors commonly obtained for Arctic and Subarctic snows with these models. But this is the first time that these models were compared with their specific snow microstructure input data for which they were defined. These results confirm first that each metric, Do as well as pc and D_{max}, must be scaled in order to minimize the RMSE between simulated and measured T_B. This aspect was discussed and partly explained in previous papers (Löwe and Picard, 2015; Roy et al., 2013; Kontu and Pulliainen, 2010). Secondly, the results show that the snow microstructure metric based on Do appears to give better results than the metric defined by D_{max} (Table 6). This may be due to the fact that microwave scattering is more directly related to Do than to D_{max}. Also, even if the shadow box used to measure D_{max}, is more accurate than visual estimates, the Do value, derived from snow SSA measurements, could give a better estimate of the effective mean size over the grain size distribution per layer than the mean value of D_{max} measurements.

It is difficult to conclude on the performance of DMRT-ML, HUT and MEMLS due to the large observed scatter on simulations, although the MEMLS model appears here slightly better for the snowpits analyzed in this study. We found a mean RMSE at high frequencies (19 and 37 GHz) of 16.6 K, 22.0 K and 23 K respectively for MEMLS_Do, DMRT-ML and HUT_D_{max}. However, as mentioned above, a specific optimization could have been made on the input parameters for each model (on the ϕ scaling factors) that would have a different effect on the models and change the results comparison. This scaling factor may also depend on the types of snow, i.e. on metamorphism processes and shape (see Löwe and Picard, 2015; Krol and Löwe, 2016). However,

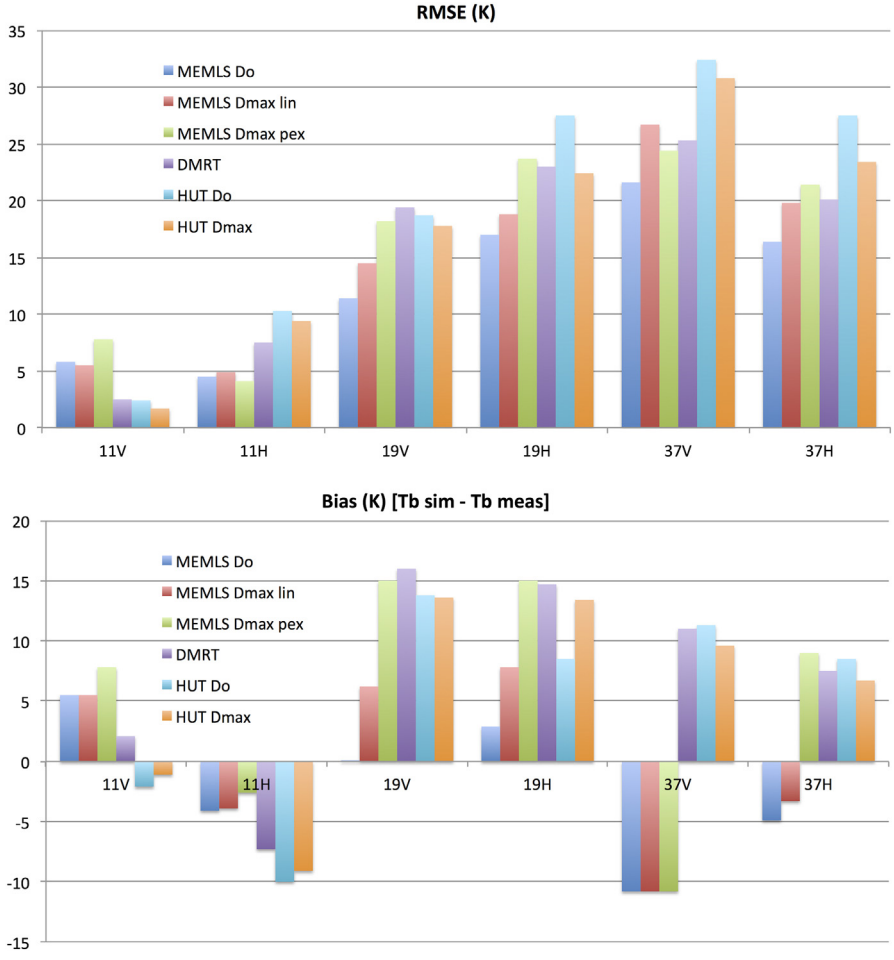

Fig. 7. Comparison between the RMSE (top) and biases (bottom) for the 6 model configurations. The corresponding values are given in Table 6.

Table 7
Comparison of linear regression parameters (coefficient of determination R^2 and slope of the regression) for simulated and measured T_B for the models shown in Fig. 6. All*: including 11 GHz at H-pol and V-pol.

Model	DMRT-ML		MEMLS						HUT			
Inputs	Do $\phi = 3.3$		Do $\phi = 1.3$		D_{max}_lin (Fig. 5)		D_{max} p_{ex} Eq. (7)		Do $\phi = 3.7$		D_{max} $\phi = 0.5$	
	R^2	Slope	R^2	Slope	R^2	Slope	R^2	Slope	R^2	Slope	R^2	Slope
19V	0.30	0.53	0.52	0.95	0.29	0.64	0.46	0.20	0.14	0.24	0.11	0.19
19H	0.13	0.33	0.23	0.47	0.17	0.39	0.03	0.12	0.05	0.18	0.05	0.17
37V	0.63	1.07	0.72	1.04	0.45	0.78	0.31	0.29	0.13	0.34	0.19	0.43
37H	0.73	1.19	0.78	1.10	0.58	0.88	0.48	0.36	0.22	0.45	0.34	0.58
All*	0.75	1.10	0.79	1.06	0.69	0.98	0.63	0.70	0.51	0.73	0.55	0.76

the comparison shown here between the four models using a synthetic snowpack (Figs. 2, 3 and 4) clearly shows the intrinsic difference in radiative transfer behavior as a function of grain size, density and ice lens variations within the snowpack, in particular for the polarization ratio (T_B H-pol/T_B V-pol).

In conclusion, to date, from a practical point of view using in-situ measurements of snow properties, this paper shows that the SSA parameter appears to be the most relevant parameter for characterizing snow microstructure, even if it must be scaled to be used for microwave simulations. Snow tomography could give more precise microstructure characterization but requires significant processing time. When suitably scaled for each model (MEMLS and DMRT-ML), the SSA parameter produces the same order of error magnitude in simulated brightness temperature. From a physical perspective, Löwe and Picard (2015) showed that MEMLS and DMRT-ML are in fact very similar.

Acknowledgements

This study was supported by the National Sciences and Engineering Research Council of Canada (NSERC), the Canadian Foundation for Innovation, Environment Canada, NASA-Goddard (L.B.) and by the Programme de développement de partenariats stratégiques en matière d'enseignement et de recherche of the Conseil franco-québécois de la coopération universitaire, a France-Québec research collaboration. The authors would like to thank Patrick Cliche and Miroslav Chum for creating the Shadow-box, all participants to the field works for their contributions to obtain the ground-based measurements, and Peter Toose and Chris Derksen (Environment Canada) for providing part of the Churchill data.

References

Armstrong, R., Brodzik, M., 2002. Hemispheric-scale comparison and evaluation of passive-microwave snow algorithms. Ann. Glaciol. 34, 38–44.
Asmus, K.W., Grant, C., 1999. Surface based radiometer (SBR) data acquisition system. Int. J. Remote Sens. 20 (15/16), 3125–3129.
Brucker, L., Picard, G., Arnaud, L., Barnola, J.M., Schneebeli, M., Brunjail, H., Lefebvre, E., Fily, M., 2011. Modeling time series of microwave brightness temperature at Dome C, Antarctica, using vertically resolved snow temperature and microstructure measurements. J. Glaciol. 57 (201), 171–182.
Champollion, N., Picard, G., Arnaud, L., Lefebvre, E., Fily, M., 2013. Hoar crystal development and disappearance at Dome C, Antarctica: observation by near-infrared photography and passive microwave satellite. Cryosphere 7:1247–1262. http://dx.doi.org/10.5194/tc-7-1247-2013.
Chang, W., Tan, S., Lemmetyinen, J., Tsang, L., Xu, X., Li, X., Yueh, S., 2014. Dense media radiative transfer applied to SnowScat and SnowSAR. IEEE J. Sel. Top. Appl. Earth Observ. Remote. Sens. 7 (9), 3811–3825.
Colbeck, S., Akitaya, E., Armstrong, R., Gubler, H., Lafeuille, J., Lied, K., McClung, D., Morris, E., 1990. The International Classification for Seasonal Snow on the Ground. Int. Commission Snow Ice Int. Assoc. Sci. Hydrol., Working Group Snow Classification, Wallingford, U.K.
Courtemanche, B., Montpetit, B., Royer, A., Roy, A., 2015. Creation of a lambertian microwave surface for retrieving the downwelling contribution in ground-based radiometric measurements. IEEE Geosci. Remote Sens. Lett. 12 (3), 462–466.
Dolant, C., Langlois, A., Montpetit, B., Brucker, L., Roy, A., Royer, A., 2016. Development of a rain-on-snow detection algorithm using passive microwave radiometry. Hydrol. Process. http://dx.doi.org/10.1002/hyp.10828 (published online in Wiley Online Library).
Domine, F., Albert, M., Huthwelker, T., Jacobi, H.W., Kokhanovsky, A.A., Lehning, M., Picard, G., Simpson, W.R., 2008. Snow physics as relevant to snow photochemistry. Atmos. Chem. Phys. 8, 171–208.
Dupont, F., Picard, G., Royer, A., Fily, M., Roy, A., Langlois, A., Champollion, N., 2014. Modeling the microwave emission of bubbly ice: applications to blue ice and superimposed ice in the Antarctic and Arctic. IEEE Trans. Geosci. Remote Sens. 52:6639–6651. http://dx.doi.org/10.1109/TGRS.2014.2299829.
Durand, M., Kim, E.J., Margulis, S.A., 2008. Quantifying uncertainty in modeling snow microwave radiance for a mountain snowpack at the point-scale, including stratigraphic effects. IEEE Trans. Geosci. Remote Sens. 46, 1753–1767.
Fierz, C., Armstrong, R.L., Durand, Y., Etchevers, P., Greene, E., McClung, D.M., Nishimura, K., Satyawali, P.K., Sokratov, S., 2009. The International Classification for Seasonal Snow on the Ground, IHP-VII Technical Documents in Hydrology, 83, IACS Contribution (1). UNESCO-IHP, Paris.
Gallet, J.-C., Domine, F., Zender, C.S., Picard, G., 2009. Measurement of the specific surface area of snow using infrared reflectance in an integrating sphere at 1310 and 1550 nm. Cryosphere 3:167–182. http://dx.doi.org/10.5194/tc-3-167-2009.
Grenfell, T.C., Putkonen, J., 2008. A method for the detection of the severe rain- on-snow event on Banks Island, using passive microwave remote sensing. Water Resour. Res. 44, W03425. http://dx.doi.org/10.1029/2007WR005929.
Grody, N., 2008. Relationship between snow parameters and microwave satellite measurements: theory compared with advanced microwave sounding unit observations from 23 to 150 GHz. J. Geophys. Res. 113:17. http://dx.doi.org/10.1029/2007JD009685.
Hallikainen, M.T., Ulaby, F.T., Van Deventer, T.E., 1987. Extinction behavior of dry snow in the 18 to 90-GHz range. IEEE Trans. Geosci. Remote Sens. 6, 737–745.
Huang, S., Tsang, L., 2012. Electromagnetic scattering of randomly rough soil surfaces based on numerical solutions of Maxwell solutions of Maxwell equations in three-dimensional simulations using a hybrid UV/PBTG/SMCG method. IEEE Trans. Geosci. Remote Sens. 50 (10), 4025–4035.
Jin, Y.Q., 1994. Electromagnetic Scattering Modelling for Quantitative Remote Sensing. Vol. 1994. World Scientific, Singapore.
Kelly, R., Chang, A., Tsang, L., Foster, J., 2003. A prototype AMSR-E global snow area and snow depth algorithm. IEEE Trans. Geosci. Remote Sens. 41 (2), 230–242.
Kontu, A., Pulliainen, J., 2010. Simulation of spaceborne microwave radiometer measurements of snow cover using in situ data and brightness temperature modeling. IEEE Trans. Geosci. Remote Sens. 48 (3), 1031–1044.
Krol, Q., Löwe, H., 2016. Relating optical and microwave grain metrics of snow: the relevance of grain shape. Cryosphere Discuss. http://dx.doi.org/10.5194/tc-2016-119.
Langlois, A., 2015. Applications of the PR Series Radiometers for Cryospheric and Soil Moisture. Research, Technical Report. Vol. 2015. © Radiometrics Corporation, p. 40.
Langlois, A., Royer, A., Montpetit, B., Picard, G., Brucker, L., Arnaud, L., Harvey-Collard, P., Fily, M., Goïta, K., 2010. On the relationship between snow grain morphology and in-situ near infrared calibrated reflectance photographs. Cold Reg. Sci. Technol. 61 (1), 34–42.
Lemmetyinen, J., Kontu, A., Rees, A., Derksen, C., Pulliainen, J.T., 2010b. Comparison of multiple layer snow emission models. Presented at the 2010 11th Specialist Meeting on Microwave Radiometry and Remote Sensing of the Environment (MicroRad). Vol. 2010, pp. 99–103 (Washington, DC).
Lemmetyinen, J., Derksen, C., Toose, P., Proksch, M., Pulliainen, J., Kontu, A., Rautiainen, K., Seppänen, J., Hallikainen, M., 2015. Simulating seasonally and spatially varying snow cover brightness temperature using HUT snow emission model and retrieval of a microwave effective grain size. Remote Sens. Environ. 156, 71–95.
Lemmetyinen, J., Pulliainen, J., Rees, A., Kontu, A., Qiu, Y., Derksen, C., 2010a. Multiple layer adaptation of the HUT snow emission model: comparison with experimental data. IEEE Trans. Geosci. Remote Sens. 48, 2781–2794.
Leppänen, L., Kontu, A., Vehviläinen, J., Lemmetyinen, J., Pulliainen, J., 2015. Comparison of traditional and optical grain size field measurements with snowpack simulations in a taiga snowpack. J. Glaciol. 61 (225), 151–162.
Lesaffre, B., Pougatch, E., Martin, E., 1997. Détermination objective des caractéristiques des grains de neige à partir d'images. La Houille Blanche 7:76–82. http://dx.doi.org/10.1051/lhb/1997068.
Liang, D., Xu, X., Tsang, L., Andreadis, K.M., Josberger, E.G., 2008. The effects of layers in dry snow on its passive microwave emissions using dense media radiative transfer theory based on the quasicrystalline approximation (QCA/DMRT). IEEE Trans. Geosci. Remote Sens. 46 (11), 3663–3671.
Liebe, H., 1989. MPM: an atmospheric millimeter-wave propagation model. Int. J. of Infrared Millimeter Waves 10 (6), 631–650.

Löwe, H., Picard, G., 2015. Microwave scattering coefficient of snow in MEMLS and DMRT-ML revisited: the relevance of sticky hard spheres and tomography-based estimates of stickiness. Cryosphere 9, 2101–2117.
Löwe, H., Riche, F., Schneebeli, M., 2013. A general treatment of snow microstructure exemplified by an improved relation for thermal conductivity. Cryosphere 7, 1473–1480.
Mätzler, C., Wiesmann, A., 2014. Microwave Emission Model of Layered Snowpacks; Documentation for MEMLS, Version 3. Institute of Applied Physics - University of Bern Sidlerstrasse 5, 3012 Bern, Switzerland, p. 26.
Mätzler C. (Ed.), P.W. Rosenkranz, A. Battaglia and J.P. Wigneron (Co-Eds.) (2006). Thermal Microwave Radiation - Applications for Remote Sensing, IET Electromagnetic Waves Series 52, (London, UK).
Mätzler, C., 2004. Notes on microwave radiation from snow samples and from a layered snowpack. IAP Research Report 96–9 Vol. 1996. University of Bern, Switzerland.
Mätzler, C., 2002. Relation between grain-size and correlation length of snow. J. Glaciol. 48, 461–466.
Mätzler, C., Wiesmann, A., 1999. Extension of the microwave emission model of layered snowpacks to coarse-grained snow. Remote Sens. Environ. 70 (3), 317–325.
Mätzler, C., 1998. Improved born approximation for scattering of radiation in a granular medium. J. Appl. Phys. 83 (11), 6111–6117.
Mätzler, C., 1994. Passive microwave signatures of landscapes in winter. Meteorog. Atmos. Phys. 54, 241–260.
Mätzler, C., 1997. Autocorrelation functions of granular media with free arrangement of spheres, spherical shells or ellipsoids. J. Appl. Phys. 81 (3), 1509–1517.
Mesinger, F., Dimego, G., Kalnay, E., Mitchell, K., Shafran, P.C., Ebisuzaki, W., et al., 2006. North American regional reanalysis. Bull. Am. Meteorol. Soc. 87 (3), 343–360.
Montpetit, B., Royer, A., Wigneron, J.-P., Chanzy, A., Mialon, A., 2015a. Evaluation of multi-frequency bare soil microwave reflectivity models. Remote Sens. Environ. 162, 186–195.
Montpetit, B., Royer, A., Roy, A., Langlois, A., 2015b. In-situ passive microwave parameterization of sub-arctic frozen organic soils. IEEE Geosci. Remote Sens. Lett. (Submitted).
Montpetit, B., Royer, A., Langlois, A., Cliche, P., Roy, A., Champollion, N., Picard, G., Domine, F., Obbard, R., 2012. New short wave infrared albedo measurements for snow specific surface area retrieval. J. Glaciol. 58 (211). http://dx.doi.org/10.3189/2012JoG11j248.
Montpetit, B., Royer, A., Roy, A., Langlois, A., Derksen, C., 2013. Snow microwave emission modeling of ice lenses within a snowpack using the microwave emission model for layered snowpacks. IEEE Trans. Geosci. Remote Sens. 51 (9), 4705–4717.
Pan, J., Durand, M., Sandells, M., Lemmetyinen, J., Kim, E.J., Pulliainen, J., Kontu, A., Derksen, C., 2016. Differences between the HUT snow emission model and MEMLS and their effects on brightness temperature simulation. IEEE Trans. Geosci. Remote Sens. 54 (4):2001–2019. http://dx.doi.org/10.1109/TGRS.2015.2493505.
Picard, G., Brucker, L., Roy, A., Dupont, F., Fily, M., Royer, A., Harlow, C., 2013. Simulation of the microwave emission of multi-layered snowpacks using the dense media radiative transfer theory: the DMRT-ML model. Geosci. Model Dev. 6:1061–1078. http://dx.doi.org/10.5194/gmd-6-1061-2013.
Picard, G., Royer, A., Arnaud, L., Fily, M., 2014. Influence of meter-scale wind-formed features on the variability of the microwave brightness temperature around Dome C in Antarctica. Cryosphere 8:1105–1119. http://dx.doi.org/10.5194/tc-8-1105-2014.
Proksch, M., Mätzler, C., Wiesmann, A., Lemmetyinen, J., Schwank, M., Löwe, H., Schneeball, M., 2016. MEMLS3&a: microwave emission model of layered snowpacks adapted to include backscattering. Geosci. Model Dev. Discuss. 8 (1–48):2015. http://dx.doi.org/10.5194/gmdd-8-1-2015 (www.geosci-model-dev-discuss.net/8/1/).
Proksch, M., Löwe, H., Schneebeli, M., 2015. Density, specific surface area, and correlation length of snow measured by high-resolution penetrometry. J. Geophys. Res. Earth Surf. 120:346–362. http://dx.doi.org/10.1002/2014JF003266.
Pulliainen, J.T., Grandell, J., Hallikainen, M.T., 1999. HUT snow emission model and its applicability to snow water equivalent retrieval. IEEE Trans. Geosci. Remote Sens. 37 (3), 1378–1390.
Riche, F., Schneebeli, M., Tschanz, S.A., 2012. Design-based stereology to quantify structural properties of artificial and natural snow using thin sections. Cold Reg. Sci. Technol. 79, 67–74.
Roy, A., Royer, A., St-Jean-Rondeau, O., Montpetit, B., Picard, G., Mavrovic, A., Marchand, N., Langlois, A., 2016. Microwave snow emission modeling uncertainties in boreal and subarctic environments. Cryosphere 10:623–638. http://dx.doi.org/10.5194/tc-10-623-2016.
Roy, V., Goita, K., Royer, A., Walker, A.E., Goodison, B.E., 2004. Snow water equivalent retrieval in a Canadian boreal environment from microwave measurements using the HUT snow emission model. IEEE Trans. Geosci. Remote Sens. 42 (9), 1850–1859.
Roy, A., Picard, G., Royer, A., Montpetit, B., Dupont, F., Langlois, A., Derksen, C., Champollion, N., 2013. Brightness temperature simulations of the Canadian seasonal snowpack driven by measurements of the snow specific surface area. IEEE Trans. Geosci. Remote Sens. 51:4692–4704. http://dx.doi.org/10.1109/TGRS.2012.2235842.
Rutter, N., Essery, R., Pomeroy, J., Altimir, N., Andreadis, K., Baker, I., Barr, A., Bartlett, P., Boone, A., Deng, H., Douville, H., Dutra, E., Elder, K., Ellis, C., Feng, X., Gelfan, A., Goodbody, A., Gusev, Y., Gustafsson, D., Hellström, R., Hirabayashi, Y., Hirota, T., Jonas, T., Koren, V., Kuragina, A., Lettenmaier, D., Li, W.-P., Luce, C., Martin, E., Nasonova, O., Pumpanen, J., Pyles, R.D., Samuelsson, P., Sandells, M., Schädler, G., Shmakin, A., Smirnova, T.G., Stähli, M., Stöckli, R., Strasser, U., Su, H., Suzuki, K., Takata, K., Tanaka, K., Thompson, E., Vesala, T., Viterbo, P., Wiltshire, A., Xia, K., Xue, Y., Yamazaki, T., 2009. Evaluation of forest snow processes models (SnowMIP2). J. Geophys. Res. - Atmos. 114. http://dx.doi.org/10.1029/2008JD011063.
Rutter, N., Sandells, M., Derksen, C., Toose, P., Royer, A., Montpetit, B., Langlois, A., Lemmetyinen, J., Pulliainen, J., 2014. Snow stratigraphic heterogeneity within ground-based passive microwave radiometer footprints: Implications for emission modeling. J. Geophys. Res. Earth Surf.:119 http://dx.doi.org/10.1002/2013JF003017.
Sandells, M., Essery, R., Rutter, N., Wake, L., Leppänen, L., Lemmetyinen, J., 2016. Microstructure representation of snow in coupled snowpack and microwave emission models. Cryosphere Discuss. http://dx.doi.org/10.5194/tc-2016-181.
Schwank, M., Rautiainen, K., Mätzler, C., Stähli, M., Lemmetyinen, J., Pulliainen, J., Vehviläinen, J., Kontu, A., Ikonen, J., Bauduin-Ménard, C., Drusch, M., Wiesmann, A., Wegmüller, U., 2014. Model for microwave emission of a snow-covered ground with focus on L band. Remote Sens. Environment 154, 180–191.
Shih, S.-E., Ding, K.-H., Kong, J.A., Yang, Y.E., Davis, R.E., Hardy, J.P., Jordan, R., 1997. Modeling of millimeter wave backscatter of time-varying snowcover. Prog. Electromagn. Res. 16, 305–330.
Tedesco, M., Kim, E.J., 2006. Intercomparison of electromagnetic models for passive microwave remote sensing of snow. IEEE Trans. Geosci. Remote Sens. 44 (10), 2654–2666.
Tsang, L., Ding, K.-H., Huang, S., Xu, X., 2013. Electromagnetic computation in scattering of electromagnetic waves by random rough surface and dense media in microwave remote sensing of land surfaces, invited review paper. Proc. IEEE TGARS 101 (2), 255–279.
Tsang, L., Kong, J.A., 2001. Scattering of Electromagnetic Waves, 3, Advanced Topics. Wiley Interscience.
Tsang, L., Pan, J., Liang, D., Li, Z., Cline, D.W., Tan, Y., 2007. Modeling active microwave remote sensing of snow using dense media radiative transfer (DMRT) theory with multiple scattering effects. IEEE Trans. Geosci. Remote Sens. 45:990–1004. http://dx.doi.org/10.1109/TGRS.2006.888854.
Wegmüller, U., Mätzler, C., 1999. Rough bare soil reflectivity model. IEEE Trans. Geosci. Remote Sens. 37 (3), 1391–1395.
Wiesmann, A., Mätzler, C., 1999. Microwave emission model of layered snowpacks. Remote Sens. Environ. 70 (3), 307–316.
Wiesmann, A., Mätzler, C., Weise, T., 1998. Radiometric and structural measurements of snow samples. Radio Sci. 33 (2), 273–289.